Physical Adsorption Analysis of Intact Supported MFI Zeolite Membranes

Karl D. Hammond,[†] Geoffrey A. Tompsett,[†] Scott M. Auerbach,*[,†,‡] and W. Curtis Conner, Jr.*[,†]

Department of Chemical Engineering, 159 Goessmann Laboratory, University of Massachusetts, Amherst, Massachusetts 01003, and Department of Chemistry, 701 Lederle Graduate Research Tower, University of Massachusetts, Amherst, Massachusetts 01003

Received November 7, 2006. In Final Form: March 1, 2007

We compare the adsorption properties of intact supported silicalite membranes with those of silicalite powder and of alumina supports using nitrogen and argon as adsorbates at 77 K. We disentangle contributions from the membrane and support and find that the support contributes significantly to the total quantity adsorbed due to its relative thickness. The micropore-filling regions of the adsorption isotherms of the powder and the supported membrane are nearly identical for the membranes studied, but the isotherms differ at higher pressures—the supported membranes exhibit a much higher quantity adsorbed than the powders. Despite this difference, no hysteresis is observed in the membrane isotherms, indicating a lack of mesoporosity (pores in the 2−50 nm range) in either membrane or support for this preparation. We estimate argon transport fluxes at steady state by assuming surface diffusion with both a constant and concentration-dependent Maxwell−Stefan diffusion coefficient in the zeolite and the support. Further, we use the respective adsorption isotherms to determine the thermodynamic correction factors—that is, the ratios of the Fick and Maxwell−Stefan diffusion coefficients—required to solve the diffusion equation. The estimated argon flux is virtually the same using adsorption data from powders and membranes. For the relatively thick supports used in our study (∼2 mm), we find that the support exerts a much greater influence on the predicted fluxes for a wide range of values of the ratio of the support to zeolite diffusion coefficients. We emphasize that the results are specific to the architecture of the supported membranes studied, and thus, the results should be interpreted accordingly.

1. Introduction

Zeolite membranes have the potential to perform energy-efficient separations of mixtures that arise in the petrochemical and fine chemical industries through their crystalline microporous structure.[1,2] Modeling transport through zeolite membranes, a necessary step in the optimization of zeolite membrane separation processes, requires accurate information about the pore sizes and equilibrium properties of real membranes,[3,4] which may contain intercrystalline defects that affect transport significantly. These defects (which in so-called "defect free" membranes do not go all the way from one surface to the other) take the form of intercrystallite void spaces and could range anywhere from a few nanometers in size to tens of nanometers. Defects in this size range, if present in sufficient quantity, should be detectable by techniques such as physical adsorption, which we explore here.

Several methods have been employed previously to determine zeolite membrane porosity and the extent of defects in membranes, including optical confocal microscopy,[5,6] electron micrographs, and mercury porosimetry.[7−17] Confocal microscopy only detects top-down or bottom-up defects and leaves dye in the pores; this dye can be removed by calcination, though this requires a second high-temperature treatment. Electron microscopy destroys the structure of the membrane (since samples must be cut to be viewed edge-on), and mercury porosimetry leaves residual mercury in the pores[18] (rendering the membrane toxic and useless for future experiments).

Physical adsorption on powders is a common method used to characterize porosity *without* causing damage to the material being analyzed.[18] Nitrogen and argon adsorption in particular have been used to determine the porosity and surface features of zeolites and other materials, including membranes.[9,19−33] Most

* To whom correspondence should be addressed. E-mail: auerbach@chem.umass.edu (S.M.A.); wconner@ecs.umass.edu (W.C.C.).

[†] Department of Chemical Engineering.

[‡] Department of Chemistry.

(1) Nair, S.; Tsapatsis, M. In *Handbook of Zeolite Science and Technology*; Auerbach, S. M., Carrado, K. A., Dutta, P. K., Eds.; Marcel-Dekker: New York, 2003, Chapter 17.

(2) Sircar, S.; Myers, A. L. In *Handbook of Zeolite Science and Technology*; Auerbach, S. M., Carrado, K. A., Dutta, P. K., Eds.; Marcel-Dekker: New York, 2003, Chapter 22.

(3) Auerbach, S. M. *Int. Rev. Phys. Chem.* **2000**, *19*, 155−198.

(4) Nelson, P. H.; Tsapatsis, M.; Auerbach, S. M. *J. Membr. Sci.* **2001**, *184*, 245−255.

(5) Bonilla, G.; Tsapatsis, M.; Vlachos, D. G.; Xomeritakis, G. *J. Membr. Sci.* **2001**, *182*, 103−109.

(6) Snyder, M. A.; Lai, Z.; Tsapatsis, M.; Vlachos, D. G. *Microporous Mesoporous Mater.* **2004**, *76*, 29−33.

(7) Larbot, A.; Julbe, A.; Guizard, C.; Cot, L. *J. Membr. Sci.* **1989**, *44*, 289−303.

(8) Sano, T.; Yanagishita, H.; Kiyozumi, Y.; Mizukami, F.; Haraya, K. *J. Membr. Sci.* **1994**, *95*, 221−228.

(9) Uzio, D.; Peureux, J.; Giroir-Fendler, A.; Dalmon, J. A.; Ramsay, J. D. F. In *Characterization of Porous Solids III*, *Stud. Surf. Sci. Catal.* **1994**, *87*, 411−418.

(10) Julbe, A.; Ramsay, J. D. F. *Membr. Sci. Technol. Ser.* **1996**, *4*, 67−118.

(11) De Vos, R. M.; Nijmeijer, A.; Keizer, K.; Verweij, H. In *Characterisation of Porous Solids IV*, *Stud. Surf. Sci. Catal.* **1997**, *213*, 675−680.

(12) Romanos, G. E.; Kikkinides, E. S.; Kanellopoulos, N. K.; Ramsay, J. D. F.; Langlois, P.; Kallus, S. In *Sixth Conference on Fundamentals of Adsorption*, *Fundamentals of Adsorption*; Giens, France, 1998; pp 1077−1082.

(13) Ramsay, J. D. F. *MRS Bull.* **1999**, *24*, 36−40.

(14) Kallus, S.; Langlois, P.; Romanos, G. E.; Steriotis, T.; Kikkinides, E. S.; Kanellopoulos, N. K.; Ramsay, J. D. F. In *Characterisation of Porous Solids V*, *Stud. Surf. Sci. Catal.* **2000**, *128*, 467−474.

(15) Ramsay, J. D. F.; Kallus, S. *Membr. Sci. Technol. Ser.* **2000**, *6*, 373−395.

(16) Kallus, S.; Condre, J. M.; Hahn, A.; Golemme, G.; Algieri, C.; Dieudonne, P.; Timmins, P.; Ramsay, J. D. F. *J. Mater. Chem.* **2002**, *12*, 3343−3350.

(17) Benito, J. M.; Conesa, A.; Rodriguez, M. A. *J. Mater. Sci.* **2005**, *40*, 6105−6112.

(18) Gregg, S. J.; Sing, K. S. W. *Adsorption, Surface Area, and Porosity*, 2nd ed.; Academic Press: London, 1982.

(19) Mintova, S.; Hölzl, M.; Valtchev, V.; Mihailova, B.; Bouizi, Y.; Bein, T. *Chem. Mater.* **2004**, *16*, 5452−5459.

10.1021/la063256c CCC: $37.00
Published on Web 06/30/2007

of these groups found detectable amounts of mesoporosity in the materials that is not present in the corresponding silicalite or silica powder; a table summarizing the results from other groups' investigations of adsorption on monolithic silicates is included in the Supporting Information. Physical adsorption presents several challenges, however, when used on membranes. Frequently, as is the case in this study, the mass of the membrane itself is not known, whereas most adsorption isotherms are plots of quantity adsorbed *per unit mass of adsorbent* against reduced pressure (P/P_0, where P_0 is the saturation pressure of the adsorbate being studied). In a zeolite membrane, there are at least *two* adsorbents (membrane, support, and possibly an intergrown layer), making the use of quantity adsorbed per unit mass of total adsorbent a complicated and less meaningful quantity. This is further complicated by the fact that the zeolite layer may not be entirely crystalline (and thus weight gain during synthesis may not be entirely accurate) and that the support may erode during synthesis. In short, we require a method to normalize the adsorption isotherm of a supported membrane, specifically to find the mass of the zeolite present in the supported membrane.

The macroscopic size of zeolite membranes also presents a challenge. In the case of powders, the powder can be inserted into a narrow-necked glass bulb which can be attached to an adsorption system. Membranes will not fit down a narrow neck, however, so other methods are required. To ensure that the membranes remain intact during the analysis, we used a specially designed stainless steel sample container that seals around the membranes after they are placed inside. We described this vessel in detail in a previous publication.[34]

Another problem presented by supported zeolite membranes is the amount of sample present during an adsorption isotherm. In the case of a powder sample, it is fairly straightforward to choose smaller or larger amounts of sample so that the amount used is optimal for obtaining reasonable signal-to-noise ratios. In an intact membrane, the amount of zeolite is often quite small, meaning more than one membrane may need to be analyzed at the same time to ensure a sufficient signal-to-noise ratio.

Permeation studies provide a complementary way to characterize zeolite membranes and provide a direct test of their performance in separations. Because flux is given by the product of velocity and *concentration*, adsorption data play a crucial role in quantitative interpretations of permeation experiments. Krishna and co-workers[35−37] have facilitated such interpretations by showing that the Maxwell−Stefan formulation of single- and multicomponent surface diffusion[38] in zeolites offers a convenient way to parametrize transport coefficients. In addition, the Maxwell−Stefan formulation offers an illustrative picture of diffusion as controlled by chemical potential gradients balanced by frictional drag forces. This approach is convenient because single-component Maxwell−Stefan diffusivities have been found to depend weakly on concentration for adsorbates that exhibit nonspecific adsorption in zeolites.[39,40] In such cases, Fick diffusivities depend strongly on loading, this dependence coming primarily from a "thermodynamic factor"[41] that can be obtained exclusively from adsorption isotherms. Because of the paucity of adsorption data for zeolite membranes, researchers typically use powder data to interpret permeation measurements. In addition, researchers often do not account for the support layer when considering transport resistances.[42] This omission is questionable, considering that support layers are normally quite thick compared to zeolite membranes (in this study, the support is thicker by a factor of about 100). In this study, we test both of these approximations by performing theoretical calculations of steady-state fluxes through zeolite membranes, armed with measured adsorption data from powders and supported membranes.

In order to make "apples-to-apples" flux comparisons using adsorption data from powders and supported membranes, we conceive of a fictional "supported powder" whose adsorption isotherm is the mass-weighted sum of powder and support isotherms. Below, we compare the permeation properties of supported membranes and powders in a variety of permeation regimes.

In this work, we compare adsorption on intact supported silicalite (MFI) membranes to adsorption on bare alumina supports and on silicalite powder. We estimate the "apparent" thickness of the membrane on the basis of the amount adsorbed in the micropore filling region, and we find that the support contributes significantly to the isotherm at high relative pressures. However, we find little mesoporosity in the supported membrane. In addition, the computed membrane fluxes show little difference between a powder and a membrane. It should be noted, however, that this result only applies to the particular silicalite membranes used in this study; membranes prepared by other methods may indeed show significant contributions to the transport that cannot be modeled with powder adsorption measurements.

In what follows, we describe the adsorption experiments we performed (Section 2), our calculations of the flux from them using both a constant and concentration-dependent Maxwell−Stefan diffusion coefficient (Section 3), and the results (Section 4). A complete discussion of the results is reserved for Section 5, after which we summarize our conclusions (Section 6).

2. Experimental Section

2.1. Zeolite Membranes and Powders. The zeolite powder used in these experiments is all-silica MFI (silicalite), Union Carbide lot 961884061002−S, calcined at 500 °C.

The membranes used in these experiments are all-silica MFI structures[43] grown on planar α-alumina substrates from the work of Nair et al.[1,44−46]

(20) Huang, L.; Wang, Z.; Sun, J.; Miao, L.; Li, Q.; Yan, Y.; Zhao, D. *J. Am. Chem. Soc.* **2000**, *122*, 3530−3531.
(21) Holland, B. T.; Abrams, L.; Stein, A. *J. Am. Chem. Soc.* **1999**, *121*, 4308−4309.
(22) Valtchev, V. *J. Mater. Chem.* **2002**, *12*, 1914−1918.
(23) Huang, L.; Wang, Z.; Wang, H.; Sun, J.; Li, Q.; Zhao, D.; Yan, Y. *Microporous Mesoporous Mater.* **2001**, *48*, 73−78.
(24) Wang, Y.; Tang, Y.; Dong, A.; Wang, X.; Ren, N.; Shan, W.; Gao, Z. *Adv. Mater.* **2002**, *14*, 994−997.
(25) Lai, R.; Gavalas, G. R. *Ind. Eng. Chem. Res.* **1998**, *37*, 4275−4283.
(26) Lai, R.; Yan, Y.; Gavalas, G. R. *Microporous Mesoporous Mater.* **2000**, *37*, 9−19.
(27) Hietala, S. L.; Smith, D. M. *Langmuir* **1993**, *9*, 249−251.
(28) Zhao, D.; Yang, P.; Melosh, N.; Feng, J.; Chmelka, B. F.; Stucky, G. D. *Adv. Mater.* **1998**, *10*, 1380−1385.
(29) Zhao, D.; Yang, P.; Chmelka, B. F.; Stucky, G. D. *Chem. Mater.* **1999**, *11*, 1174−1178.
(30) Yanazawa, H.; Hironori, M.; Itoh, H.; Nakai, K.; Suzuki, I. *J. Vac. Sci. Technol. B* **2002**, *20*, 1883−1835.
(31) Bartels, O.; Zukal, A. *J. Mater. Sci.* **2005**, *40*, 2603−2605.
(32) Chao, K.-J.; Liu, P.-H.; Huang, K.-Y. *C. R. Chim.* **2005**, *8*, 727−739.
(33) Zhang, J.; Palaniappan, A.; Su, X. D.; Tay, F. E. H. *Appl. Surf. Sci.* **2005**, *245*, 304−309.
(34) Hammond, K. D.; Tompsett, G. A.; Auerbach, S. M.; Conner, W. C. *J. Porous Mater.* **2007** (available online, DOI 0.1007/s10934-006-9034-x).
(35) Kapteijn, F.; Moulijn, J. A.; Krishna, R. *Chem. Eng. Sci.* **2000**, *55*, 2923−2930.
(36) Krishna, R.; Paschek, D. *Chem. Eng. J.* **2002**, *87*, 1−9.
(37) Krishna, R.; van Baten, J. M. *J. Phys. Chem. B* **2005**, *109*, 6386−6396.
(38) Krishna, R.; Wesselingh, J. A. *Chem. Eng. Sci.* **1997**, *52*, 861−911.
(39) Maginn, E. J.; Bell, A. T.; Theodorou, D. N. *J. Phys. Chem.* **1993**, *97*, 4173−4181.
(40) Krishna, R. In *Handbook of Zeolite Science and Technology*; Auerbach, S. M., Carrado, K. A., Dutta, P. K., Eds.; Marcel-Dekker: New York, 2003, Chapter 23.
(41) Kärger, J.; Vasenkov, S.; Auerbach, S. M. In *Handbook of Zeolite Science and Technology*; Auerbach, S. M., Carrado, K. A., Dutta, P. K., Eds.; Marcel-Dekker: New York, 2003, Chapter 10.
(42) Ramanan, H.; Auerbach, S. M.; Tsapatsis, M. *J. Phys. Chem. B* **2004**, *108*, 17179−17187.

The supports were formed using calcined alumina (A16SG, Alcoa Chemicals) pressed into 22 mm discs and fired for 30 h at 800 °C followed by 24 h at 1180 °C. The silicalite was grown by a secondary (seeded) growth procedure as described by Xomeritakis et al.[44] The membranes were calcined to ensure that any organic molecules were removed by ramping the air temperature at about one degree per minute over the course of 8 h to 525 °C. That temperature was maintained for five more hours, then the temperature was ramped down at the same rate back to ambient temperature. The supports were polished with SiC sandpaper on the growth surface before the synthesis procedure.[45]

2.2. X-ray Diffraction. Powders and membranes were analyzed using a Philips X'Pert diffractometer using Cu K_α X-rays with a wavelength of 1.64 Å. A slit width of 1° on the source and detector was used and scans from $2\theta = 5°$ to 50° were obtained at a rate of 0.01°/s. The diffraction patterns (see Supporting Information) show that the crystals have a primary out-of-plane orientation either along the *c* axis (00*l* crystal face) or along the *h*0*h* crystal faces (see ref 47). The straight channels of MFI run along the *b* axis (0*k*0 face), while the zigzag channels run along the *a* axis (*h*00 face).

2.3. Electron Microscopy. Scanning electron micrographs of a membrane were obtained using a JEOL 7401F scanning electron microscope (SEM). Samples were prepared by vertically mounting a broken membrane disc on an aluminum sample stub using carbon adhesive tape. We broke the disc for analysis by applying a sudden mechanical stress and did not use it for subsequent adsorption analysis. Samples were dried in a desiccant box prior to evacuation in the SEM. No coating was applied. Magnifications of 10 000−100 000 were used in the micrographs. The membrane thickness for that particular membrane appears to be ∼5 μm, as can be seen in Figure 1. At higher magnification, we can see grain boundaries between the MFI crystals; the grain boundaries appear to be on the order of 10 nm or smaller (Figure 1). Note that the support is on the order of 100× thicker than the membrane.

2.4. Adsorption. *2.4.1. Sample Container.* While the standard glass adsorption cell has been adequate to study vapor adsorption in zeolite *powders*, it presents problems when measuring adsorption in zeolite *membranes* for the simple reason that the membranes are too big to fit down the neck of the sample cell. We designed a new sample container for measuring physical adsorption in membranes, which we have described in detail in ref 34. The procedures we described in that article to seal and support the container were followed when measuring sorption isotherms for this work. The container employs a resealable 2 1/8 in. stainless steel Conflat flange (MDC Vacuum Products) attached to a 1/4 in. glass tube via a glass-to-metal seal. The glass tube can be attached to an adsorption system using existing fittings.

2.4.2. Sample Preparation. We evacuated the samples for sorption analysis using a roughing pump and an oil-free turbomolecular pump to draw vacuum to the rated residual pressure of 10^{-9} Torr (10^{-7} Pa or 10^{-12} atm). We heated each sample over the course of five or more hours to 300−350 °C, which we maintained for 1−4 days to remove water and other adsorbed materials from the membranes. The samples were cooled to room temperature over the course of about 5 h, and then the temperature was lowered to the bath temperature (−196 °C) over the course of a further 3−4 h. We used this slow heating/cooling cycle to minimize mechanical stress due to the differences in thermal expansion properties between the membrane and the support.[48−50]

2.4.3. Adsorption−Desorption System. Adsorption and desorption isotherms were measured at the normal boiling point of nitrogen (77 K) using an AUTOSORB-1-MPC (Quantachrome Instruments; Boynton Beach, FL) gas adsorption system or our own high-resolution adsorption equipment, as detailed in refs 51 and 52. Nitrogen and argon were used as adsorbates, and a constant level of the liquid nitrogen bath was maintained during all measurements. Dead space measurements were conducted using helium; saturation pressures were determined by condensing/subliming adsorbate in a separate vessel inside the cryogenic bath at intervals throughout the experiment or by condensing/subliming adsorbate in the sample container at the end of the experiment. All gases used in the experiments are ultrahigh purity (Merriam-Graves Corporation; Charlestown, NH).

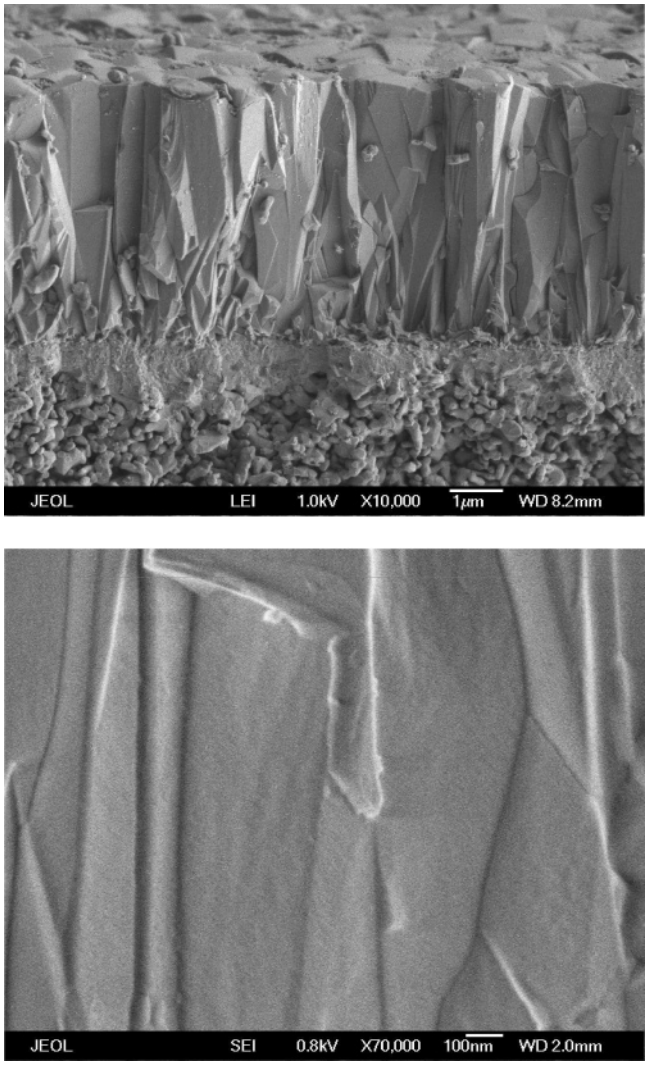

Figure 1. Scanning electron micrographs of an *h*0*h*-oriented MFI membrane. Top: 10 000× magnification showing the zeolite layer (top) and the porous alumina substrate. Bottom: 70 000× magnification showing crystal intergrowth pores.

3. Transport Calculations

3.1. General Formulation. As discused in the Introduction, adsorption measurements play an important role in interpreting fluxes and selectivities for permeation through zeolite membranes. Many researchers use powder adsorption data to interpret membrane fluxes because of the difficulties (discussed in the

(43) International Zeolite Association, *Database of Zeolite Structures*, http://www.iza-structure.org/databases.
(44) Xomeritakis, G.; Gouzinis, A.; Nair, S.; Okubo, T.; He, M.-Y.; Overney, R. M.; Tsapatsis, M. *Chem. Eng. Sci.* **1999**, *54*, 3521−3531.
(45) Xomeritakis, G.; Nair, S.; Tsapatsis, M. *Microporous Mesoporous Mater.* **2000**, *38*, 61−73.
(46) Nair, S. Ph.D. dissertation, University of Massachusetts Amherst, 2002.
(47) Lai, Z.; Bonilla, G.; Diaz, I.; Nery, J. G.; Sujaoti, K.; Amat, M. A.; Kokkoli, E.; Terasaki, O.; Thompson, R. W.; Tsapatsis, M.; Vlachos, D. G. *Science* **2003**, *300*, 456−460.
(48) Dong, J.; Wegner, K.; Lin, Y. *J. Membr. Sci.* **1998**, *148*, 233−241.
(49) Dong, J.; Lin, Y. S.; Hu, M. Z.-C.; Peascoe, R. A.; Payzant, E. A. *Microporous Mesoporous Mater.* **2000**, *34*, 241−253.
(50) Jeong, H.-K.; Lai, Z.; Tsapatsis, M.; Hanson, J. *Microporous Mesoporous Mater.* **2005**, *84*, 332−337.
(51) Conner, W. C. *Apparatus and method for efficient determination of equilibrium adsorption isotherms at low pressures*, U.S. Patent 5,637,810, 1995.
(52) Vallee, S. J.; Conner, W. C. *J. Phys. Chem. B* **2006**, *110*, 15459−15470.

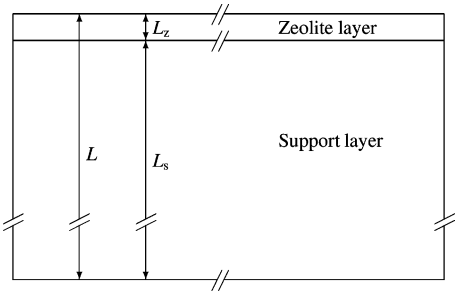

Figure 2. Diagram of the zeolite/support regions as used in our calculations. Please note that this is not to scale: the zeolite is actually *much* thinner relative to the support than can be shown here.

Introduction) in collecting such data for intact membranes. To gauge the errors associated with such a practice, we calculate steady-state permeation fluxes using both powder and membrane adsorption data, as reported later in this article. Because our membranes are supported, the correct comparison is between fluxes from supported membranes and "supported powders"—composites of a support and a zeolite powder. We assume that membrane permeation is controlled by surface diffusion and apply Fick's law for one-dimensional steady-state diffusion as given by[41]

$$\frac{dN}{dx} = \frac{d}{dx}\left(-D\frac{dC}{dx}\right) = 0 \tag{1}$$

where N is the transmembrane flux, x is the transmembrane position coordinate, D is the Fick diffusion coefficient, and C is the concentration. When applying the spatial derivative d/dx, we account for the dependence of the Fick diffusion coefficient on concentration, which in turn depends on position. We do this by writing D in terms of the Maxwell−Stefan diffusion coefficient ($Đ$)[38,41] according to $D = Đ\Gamma$, where Γ is the thermodynamic factor given by

$$\Gamma = \left(\frac{\partial \log f}{\partial \log C}\right)_T \tag{2}$$

In eq 2, T is temperature and f is the fugacity of the external vapor phase. The vapor phase is nearly ideal under the low-pressure conditions we study, which allows us to replace f with the pressure, P. The thermodynamic factor can be extracted from isotherm data as discussed in Section 3.2. This method for estimating the primary concentration dependence of D is convenient because $Đ$ has been found to depend weakly on concentration for adsorbates that exhibit nonspecific adsorption in zeolites,[39] as is expected for nitrogen and argon in silicalite. As such, in this section we estimate the concentration dependence of the Fick diffusivity exclusively from the adsorption data reported below. We also consider the situation where $Đ$ depends on concentration in Section 3.4.

For the case of a loading-independent Maxwell−Stefan diffusion coefficient, eq 1 takes the form

$$Đ\left[\frac{d\Gamma}{dC}\left(\frac{dC}{dx}\right)^2 + \Gamma\left(\frac{d^2C}{dx^2}\right)\right] = 0 \tag{3}$$

Equation 3 indicates that the input is Γ as a function of C and the output solution is the concentration profile $C(x)$. Equation 3 also clearly indicates that the concentration profile $C(x)$ is independent of $Đ$, though the magnitude of the steady-state flux N is proportional to $Đ$. Equation 3 is subject to several boundary conditions: at the inflow (high pressure) side, at the outflow (low pressure) side, and at the interface between zeolite and support. We consider both permeation directions: (*i*) inflow on the zeolite side of the membrane and (*ii*) inflow on the support side. In general, we assume local thermodynamic equilibria on both external edges of the supported membrane. This is equivalent to assuming that adsorption/desorption processes are faster than diffusion through the membrane, which is valid in the limit of relatively thick membranes. For simplicity, we assume that the outflow side is at zero pressure. Distinguishing now between zeolite (z) and support (s) regions (see Figure 2), which exhibit significantly different adsorption/diffusion properties, the diffusion equation becomes

$$\frac{d\Gamma_z}{dC_z}\left(\frac{dC_z}{dx}\right)^2 + \Gamma_z\left(\frac{d^2C_z}{dx^2}\right) = 0 = \frac{d\Gamma_s}{dC_s}\left(\frac{dC_s}{dx}\right)^2 + \Gamma_s\left(\frac{d^2C_s}{dx^2}\right) \tag{4}$$

subject to the boundary conditions:

$$N_z = -Đ_z\Gamma_z\left.\frac{dC_z}{dx}\right|_{x=x_{int}} = -Đ_s\Gamma_s\left.\frac{dC_s}{dx}\right|_{x=x_{int}} = N_s = N \tag{5}$$

$$C_z(x_{int}) = C_z^{ads}(T, P_z(x_{int})) \tag{6a}$$

$$C_s(x_{int}) = C_s^{ads}(T, P_s(x_{int})) \tag{6b}$$

$$P_z(x_{int}) = P_s(x_{int}) \tag{6c}$$

$$C_{z-edge} = C_z^{ads}(T, P_{z-edge}) \tag{7a}$$

$$C_{s-edge} = C_s^{ads}(T, P_{s-edge}) \tag{7b}$$

where x_{int} is the location of the membrane−support interface, P_{z-edge}/P_{s-edge} are the pressures on zeolite/support edges, C_{z-edge}/C_{s-edge} are the adsorbate concentrations on zeolite/support edges, and $C_z^{ads}(T, P)/C_s^{ads}(T, P)$ are the equilibrium concentrations in the zeolite/support as functions of T and P. Equations 5 and 6 enforce the constancy of flux and pressure at the zeolite−support interface, while eq 7 enforces local thermodynamic equilibrium. Please note that eq 6 is used as follows. The pressure at the interface is *defined* by eq 6a or 6b, depending on which side of the membrane is at vacuum. The concentration at the other side of the interface is then determined from eq 6b or 6a, using eq 6c as the boundary condition.

3.2. Experimental Inputs. We now recast these equations in a form more suitable to actual adsorption data, since these data ultimately determine the calculated concentration profiles. We typically measure $\hat{V}_{ads}$, the standard volume of gas adsorbed per unit mass of zeolite. As such, the concentration is given by

$$C = \rho_z(\hat{n}_{ads}/\hat{V}_{ads})\hat{V}_{ads} \tag{8}$$

where ρ_z is the mass density of the zeolite, and the ratio $\hat{n}_{ads}/\hat{V}_{ads}$ is equal to the standard molar density of an ideal gas, i.e., $P^{\ominus}/RT^{\ominus} = 40.9$ mol/m^3. Using this relationship, several constants can be eliminated from the differential equations. For convenience, we also add a constant inside the derivative that defines the thermodynamic correction factor. We choose this constant to be the logarithm of the saturation pressure, P_0, since the quantity P/P_0 is the value we actually report. Using these simplifications, we write the thermodynamic correction factor as follows

$$\Gamma = \frac{\partial \log P}{\partial \log C} = C\frac{\partial \log P}{\partial C}$$
$$= \left(\rho_z \frac{P^\ominus}{RT^\ominus}\hat{V}_{ads}\right)\frac{\partial(\log P - \log P_0)}{\partial\left(\rho_z \frac{P^\ominus}{RT^\ominus}\hat{V}_{ads}\right)} = \frac{\partial \log (P/P_0)}{\partial \log \hat{V}_{ads}} \quad (9)$$

The last term in eq 9 is calculated directly from our measured adsorption isotherms. Expressing the flux in these same variables gives

$$N = -D\frac{dC}{dx} = -\mathcal{D}\Gamma\frac{d}{dx}\left(\rho_z \frac{P^\ominus}{RT^\ominus}\hat{V}_{ads}\right) = -\rho_z\left(\frac{P^\ominus}{RT^\ominus}\right)\mathcal{D}\Gamma\frac{d\hat{V}_{ads}}{dx} \quad (10)$$

with Γ expressed in eq 9. Equation 10 suggests the definition of a reduced flux, N^*, given by

$$N^* = \frac{NL_r RT^\ominus}{\rho_z \mathcal{D}P^\ominus} \quad (11)$$

As such, N^* is simply given by $\Gamma(d\hat{V}_{ads}/dx^*)$, where $x^* = x/L_r$ is the scaled transmembrane coordinate and L_r is the width of the region (either the zeolite or the support). This scaled flux has units of $\hat{V}_{ads}$, namely, volume per unit mass of zeolite.

To solve for the concentration profile $\hat{V}_{ads}(x^*)$ and hence for N^*, we use centered-differencing ($\mathcal{O}(h^2)$) methods to discretize the scaled version of eq 4 using different mesh densities in the zeolite and support regions, because the zeolite is much thinner than the support. At the endpoints, we used a one-sided ($\mathcal{O}(h^2)$) finite difference formula instead of a centered one. We solved the problem on the vacuum side first (zeolite or support), then matched the solution on the inflow (feed) side. The discretized *residual*, $\vec{r}$, of the problem is thus

$$r_j = \left(\frac{d\Gamma}{d\hat{V}}\right)_j\left(\frac{\hat{V}_{j+1} - \hat{V}_{j-1}}{2h}\right)^2 + \Gamma_j\left(\frac{\hat{V}_{j+1} - 2\hat{V}_j + \hat{V}_{j-1}}{h^2}\right) \quad (12)$$

where r_j is element j of the residual vector and h is the spacing between elements on the x axis. The terms Γ_j and $(d\Gamma/d\hat{V})_j$ are determined by centered difference methods from the measured isotherms; the values are interpolated linearly to the value of $\hat{V}_j$, the value of $\hat{V}_{ads}$ at point $x = hj$ in space. We minimize the norm of this residual vector in each region (zeolite and support) with Newton's Method[53] by solving the following linear system at each iteration

$$J\cdot\vec{\delta} + \vec{r} = \vec{0} \quad (13)$$

where J is the Jacobian ($J_{ij} = \partial r_i/\partial \hat{V}_j$), and then updating the volume-adsorbed vector at each iteration k by $\hat{V}_j[k+1] = \hat{V}_j[k] + \delta_j$. The linear system is tridiagonal and thus can be solved with a routine such as that found in ref 54, which we employed in this work. This procedure is repeated until $||\vec{r}||$ is smaller than a certain tolerance (in this case, usually 10^{-5} cm^3 STP).

As discussed above, comparing transport through supported membranes and "supported powders" is the correct way to gauge the impact of using powder data to interpret membrane permeation. Implementing the separation of the transport problem for "supported powders" is straightforward because powder and support adsorption data are obtained separately. However, implementing the separation of the transport problem for supported zeolite membranes is less straightforward. To isolate adsorption data in the zeolite membrane, we computed the difference between the composite isotherm of zeolite plus support and the isotherm of the support only. At high relative pressures, the resulting membrane-only isotherm shows unphysical properties, namely, that the adsorbed amount decreases with increasing relative pressure (cf. Figure 12). This would make $\Gamma < 0$, which would produce flux in the same direction as the chemical potential gradient, which violates the Second Law of Thermodynamics. Because this occurs at pressures that essentially saturate the zeolite micropores, we replace the decreasing isotherm with a very slightly increasing function, as shown in Figure 12. In some cases, this increases numerical error in the solution, as will be seen below.

Table 1. Cases Examined in Flux Calculations[a]

figure	symbol	isotherm	$\mathcal{D}_z$ (m^2/s)	zeolite location
N/A	N/A	powder	7.5×10^{-7}	vacuum[b]
14	○	powder	7.5×10^{-7}	feed
N/A	N/A	membrane	7.5×10^{-7}	vacuum[b]
14	●	membrane	7.5×10^{-7}	feed
N/A	N/A	powder	1.2×10^{-7}	vacuum[b]
14	◇	powder	1.2×10^{-7}	feed
N/A	N/A	membrane	1.2×10^{-7}	vacuum[b]
14	♦	membrane	1.2×10^{-7}	feed
13	□	powder	7.5×10^{-10}	vacuum
14	□	powder	7.5×10^{-10}	feed
13	■, ♦	membrane	7.5×10^{-10}	vacuum
14	■	membrane	7.5×10^{-10}	feed
13	△	powder	7.5×10^{-13}	vacuum
14	△	powder	7.5×10^{-13}	feed
13	▲, ▼	membrane	7.5×10^{-13}	vacuum
14	▲	membrane	7.5×10^{-13}	feed

[a] $\mathcal{D}_s = 7.5 \times 10^{-7}$ m^2/s in all cases. [b] The calculations for cases where the zeolite membrane is at vacuum and the diffusion coefficients are of the same order of magnitude require a feed pressure so close to saturation to achieve any adsorption at all in the zeolite that no flux could be calculated. Accordingly, these cases are not plotted.

3.3. Parametrization. To predict actual fluxes, we need to specify numerical values for density, thickness, and Maxwell−Stefan diffusion coefficient in both zeolite and support regions. We assume the density of silicalite to be 1.76 g/cm^3 as reported in ref 55, and the density of the support to be the same as the density of the overall disc, which we measure to be 1.91 g/cm^3 on the basis of total weight and volume. We estimate the thickness of the zeolite layer, L_z, to be ~5 μm from Figure 1, and we determined the total thickness of the membrane and support, L, to be 1.984 mm from measurements using a caliper. The total thickness of the support is thus 1.979 mm. We fixed $\mathcal{D}_s$ at 7.5×10^{-7} m^2/s, the value for bulk liquid nitrogen at 77 K.[56] We set $\mathcal{D}_z$ to four different values: $\mathcal{D}_s$, 0.16 $\mathcal{D}_s$ (a value chosen on the basis of differences found for self-diffusion in carbon micropores[56]), 10^{-3} $\mathcal{D}_s$, and 10^{-6} $\mathcal{D}_s$. We studied this range of values of $\mathcal{D}_z$ to explore whether the impact of using powder vs membrane adsorption data is influenced by the relative diffusivities in the problem. With these four values of $\mathcal{D}_z$, the two permeation directions, and the comparison between powder and membrane adsorption data, we considered a total of 16 different transport systems, which are summarized in Table 1.

3.4. Alternate Formulation. We have assumed that the "corrected" diffusivity, $\mathcal{D}$, is a constant up to this point.

(53) Chun, C.; Ham, Y. *Commun. Numer. Methods Eng.* **2006**, *22*, 475−487.
(54) Press, W. H.; Flannery, B. P.; Teukolsky, S. A.; Vetterling, W. T. *Numerical Recipes: The Art of Scientific Computing*; Cambridge University Press: Cambridge, 1986.
(55) Szostak, R. *Handbook of Molecular Sieves: Principles of Synthesis and Identification*, 2nd ed.; Springer: London, 1992.
(56) Sweatman, M. B.; Quirke, N. *Langmuir* **2001**, *17*, 5011−5020.

However, simulations[57,58] have predicted that the Maxwell−Stefan diffusion coefficient decreases with loading for argon adsorption in silicalite at standard temperature. An approximate fit of the results of Skoulidas and Sholl[57] indicates a function of the form

$$Đ(C) = Đ_0[\alpha + (1 - \alpha)\, e^{-C/C_{ref}}] \quad (14)$$

can describe the concentration dependence of $Đ$ for argon. This function is monotonically decreasing but remains positive for all concentrations. Though our use of this function is inspired by a particular system (argon at standard temperature in silicalite), our goal in using it is to determine in a general, qualitative way the impact of a loading-dependent Maxwell−Stefan diffusivity on our comparisons.

Accounting for a concentration dependence of $Đ$ requires us to generalize eq 3, which becomes

$$Đ\frac{d\Gamma}{dC}\left(\frac{dC}{dx}\right)^2 + \Gamma\frac{dĐ}{dC}\left(\frac{dC}{dx}\right)^2 + Đ\Gamma\left(\frac{d^2C}{dx^2}\right) = 0 \quad (15)$$

The second term of this equation arises from the concentration dependence of the diffusion coefficient. We account for this by using the volume adsorbed in a variant on eq 14. We chose parameters such that the diffusivity changed as a function of $\hat{V}_{ads}$ in a manner consistent with the results of Skoulidas and Sholl[57] with the diffusivity near satuaration ($P/P_0 = 1$) decreasing to 80% of its value at infinite dilution ($P/P_0 = 0$). We also studied another case with a more extreme concentration dependence (eq 16b) to explore how weak and strong loading dependencies impact the powder−membrane flux comparisons. The weak and strong functions were chosen to be

$$Đ = Đ_0[0.8 + 0.2\, e^{-\hat{V}_{ads}/60}] = Đ_0F_1(\hat{V}_{ads}) \quad (16a)$$

$$Đ = Đ_0[0.2 + 0.8\, e^{-\hat{V}_{ads}/60}] = Đ_0F_2(\hat{V}_{ads}) \quad (16b)$$

with $\hat{V}_{ads}$ in units of cm^3 STP/g. The function F is used to represent the concentration dependence of $Đ$ itself.

With these new definitions, the flux is now given by

$$N = -D\frac{dC}{dx} = -\rho_z\left(\frac{P^\ominus}{RT^\ominus}\right)Đ_0F\Gamma\frac{d\hat{V}_{ads}}{dx} \quad (17)$$

and the reduced flux, N^*, is now given by

$$N^* = \frac{NL_tRT^\ominus}{\rho_z Đ_0 P^\ominus} \quad (18)$$

with other definitions being the same as those given in Section 3.2.

The residual of the discretized problem, with F_j representing the value of $F(\hat{V}_{ads})$ at $\hat{V}_{ads} = \hat{V}_j$, is

$$r_j = F_j\left(\frac{d\Gamma}{d\hat{V}}\right)_j\left(\frac{\hat{V}_{j+1} - \hat{V}_{j-1}}{2h}\right)^2 + \Gamma_j\left(\frac{dF}{d\hat{V}}\right)_j\left(\frac{\hat{V}_{j+1} - \hat{V}_{j-1}}{2h}\right)^2 + F_j\Gamma_j\left(\frac{\hat{V}_{j+1} - 2\hat{V}_j + \hat{V}_{j-1}}{h^2}\right) \quad (19)$$

(57) Skoulidas, A. I.; Sholl, D. S. *J. Phys. Chem. A* **2003**, *107*, 10132−10141.
(58) Beerdsen, E.; Dubbeldam, D.; Smit, B. *J. Phys. Chem. A* **2006**, *110*, 22754−22772.

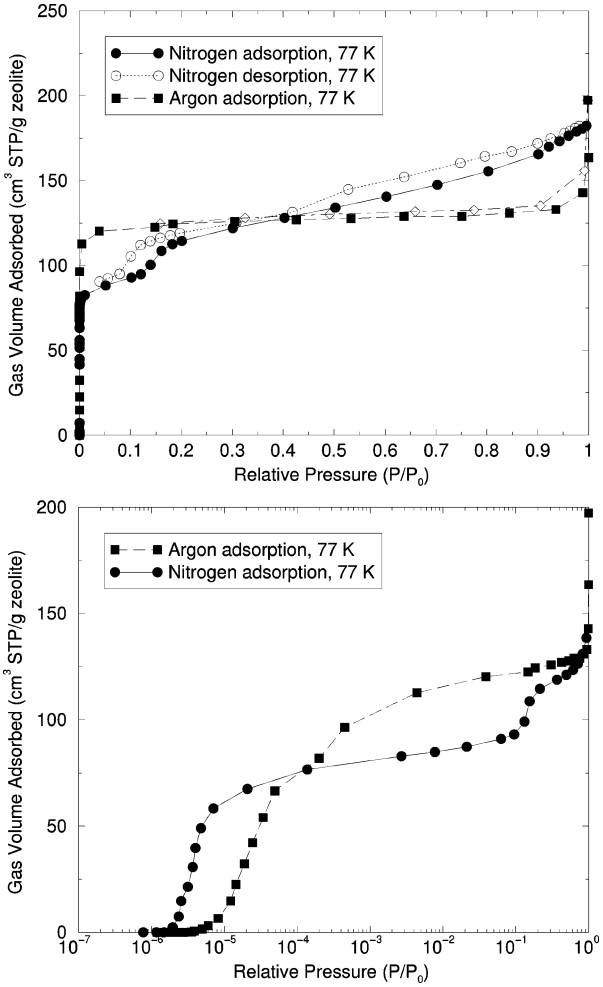

Figure 3. Adsorption isotherms of silicalite powder at 77 K using nitrogen (circles) and argon (squares) as the adsorbate. Filled symbols represent adsorption points; empty symbols represent desorption points. A logarithmic scale is used in the bottom figure to show the micropore adsorption region and a linear scale is used in the top to show standard adsorption (lines are drawn to guide the eye). Note that the desorption branches have been omitted in the bottom figure for clarity, and that the apparent hysteresis that closes at $P/P_0 \approx 0.42$ is due to the tensile strength effect[18] and the processing of the powder.

The Jacobian is still a tridiagonal matrix, with extra terms containing F_j, $(dF/d\hat{V})_j$ and $(d^2F/d\hat{V}^2)_j$ appearing on the diagonal in addition to those involving Γ and its derivatives.

We have only considered the case of *h*0*h*-oriented membranes and silicalite powder for calculations involving a concentration-dependent diffusion coefficent, as that is sufficient to demonstrate its effects.

4. Results

4.1. Adsorption Isotherms. *4.1.1. Reference Systems.* We chose two systems to serve as references with which to compare membrane adsorption isotherms: silicalite powder and fired alumina supports as described herein. We hypothesize that a membrane's adsorption properties in the low-pressure region of the isotherm should be very similar to those of a powder sample in the same region ($<10^{-5}$ in relative pressure for nitrogen, $<10^{-4}$ for argon). This is based on the assumption that the measured micropore volume of a supported zeolite membrane should not be affected by the support if the support is not microporous. In the higher-pressure regions, corresponding to meso- and macropore adsorption and surface coverage, we expect total adsorption to

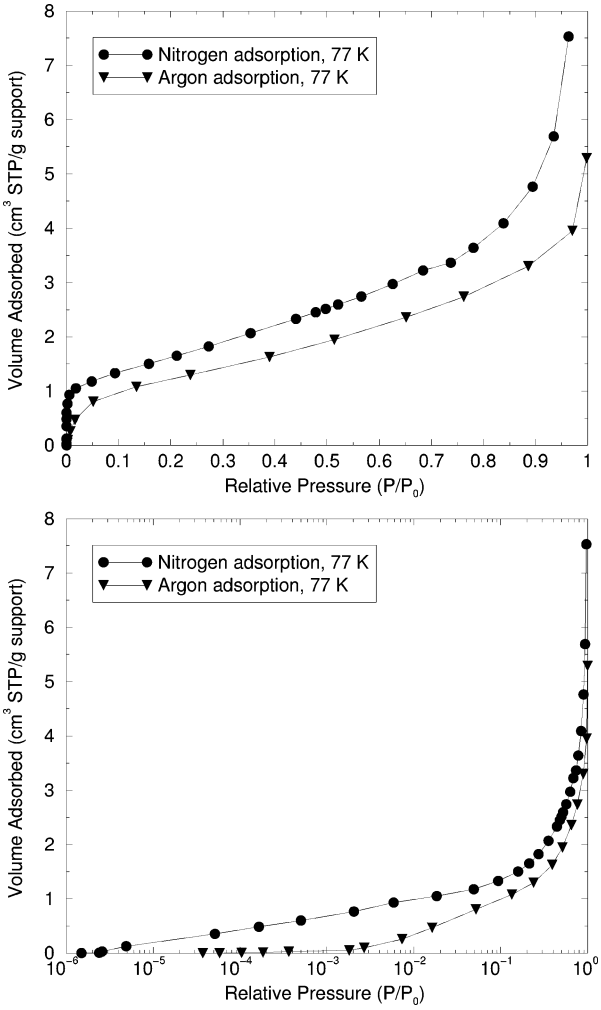

Figure 4. Adsorption isotherms of planar supports at 77 K. Triangles indicate argon adsorption, and circles indicate nitrogen adsorption. The support's lack of microporosity is revealed by the lack of adsorption in the low-pressure region (below 10^{-4} relative pressure). The top figure uses a linear scale, while the bottom figure uses a logarithmic scale. No hysteresis is observed in the desorption isotherm (not shown).

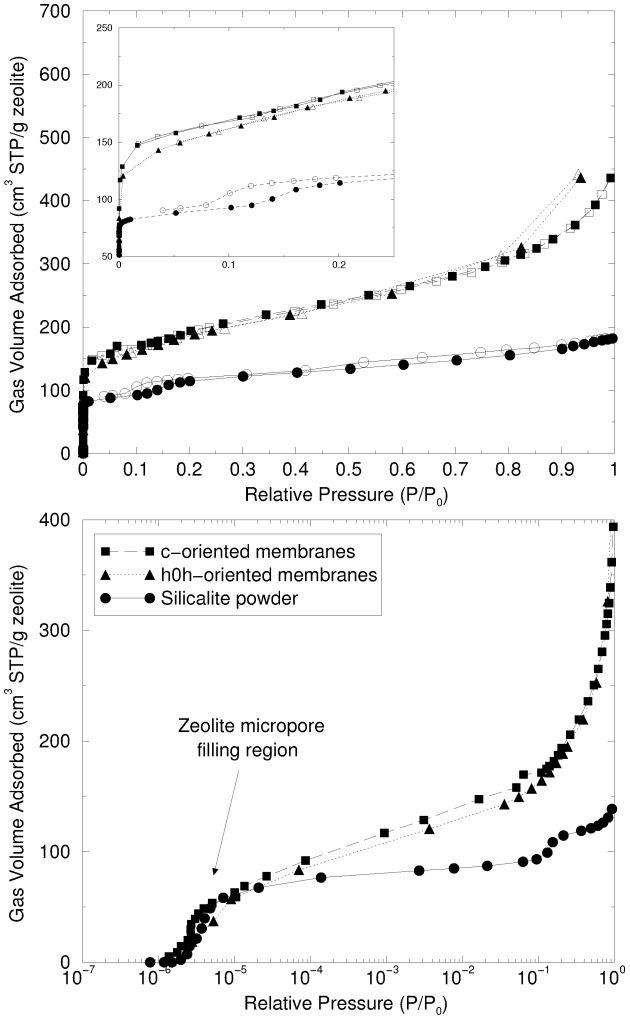

Figure 5. Comparison of nitrogen isotherms at 77 K for silicalite powder (○), *h*0*h*-oriented silicalite membranes (▲), and *c*-oriented silicalite membranes (■) using mass m_I (obtained by matching the adsorption of membrane and support to powder at the pressure when the micropores are filled). Both linear (top) and logarithmic (bottom) pressure scales are shown. Filled symbols represent adsorption points; open symbols represent desorption. Inset: expansion of low-pressure hysteresis region showing powder sorption along with sorption on *c*- and *h*0*h*-oriented membranes.

be sensitive to the difference between powder and membrane microstructures and to be more influenced by the support. Our reference isotherms are shown in Figures 3−4.

4.1.2. Membrane Adsorption. Isotherms of the membrane samples were collected in a similar fashion to those of the supports. In addition, the sample heating and cooling rates were more carefully controlled to avoid damage to the supported membrane, as discussed in ref 34.

As mentioned in the Introduction, the choice of normalization parameters (typically the mass of the zeolite is used) is a problem in membrane adsorption. The mass of the entire supported membrane can be determined by weighing, and the mass of zeolite powder can be determined in the same manner. The masses of membrane and support, however, are not as simple to obtain. A first estimate is to weigh the support before and after the synthesis procedure; the excess mass is presumed to be the mass of the zeolite. This becomes inaccurate if the support's exact mass was not known at synthesis time, if the support eroded during the synthesis procedure, and/or if the deposited material is not entirely crystalline. It should be noted that the synthesis is performed under alkaline conditions (pH ≈ 12), at which silica and alumina are likely to dissolve to some extent.

As mentioned in the Introduction, we did not know the mass of the support prior to membrane synthesis. To determine the amount of zeolite present in the supported membranes we analyzed, we compared the isotherms of the MFI membranes to the isotherms of MFI powder (Figures 5−8). From this comparison, we scaled the vertical axis of the isotherm by a mass parameter so that the quantity adsorbed *per gram zeolite* is the same as that for silicalite powder in a specific region.

We chose two regions of the isotherm to use for mass estimation: (I) scaling the zeolite mass so that the membrane isotherm matches the powder isotherm (Figure 3) at $P/P_0 = 8 \times 10^{-6}$ (N_2) or $P/P_0 = 6 \times 10^{-5}$ (Ar), hereafter referred to as the *micropore adsorption point* (where the isotherm starts to level off); (II) scaling the zeolite mass so that the membrane isotherm matches the sum of the powder isotherm (Figure 3) and the support isotherm (Figure 4) in the range $P/P_0 \in (10^{-4}-10^{-2})$, which we chose because no pores would be expected to fill in that region. We call these masses m_I and m_{II}, respectively. A comparison of the two methods is shown in Table 2.

As can be seen in Figures 5−8, the two methods yield isotherm characteristics that are not identical. Method (I) seems to be

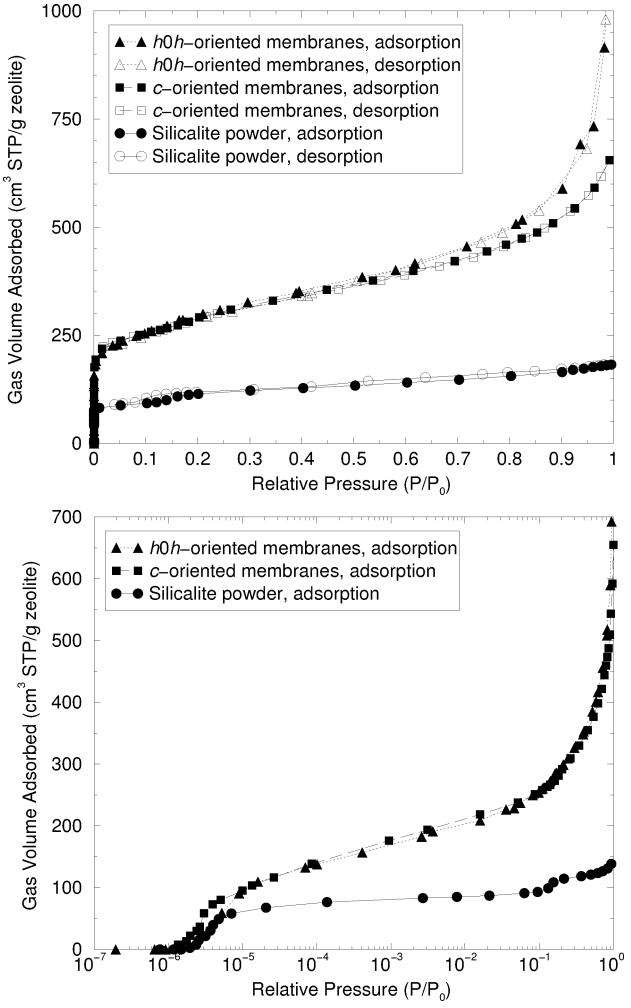

Figure 6. Comparison of nitrogen adsorption isotherms at 77 K for silicalite powder (●), *h*0*h*-oriented silicalite membranes (▲), and *c*-oriented silicalite membranes (■) using mass m_{II} (obtained by matching the adsorption of membrane and support to powder and support in the region between micropore filling and $P/P_0 = 0.1$). Both a linear (top) and logarithmic (bottom) pressure scale are shown. Filled symbols represent adsorption points; open symbols represent desorption.

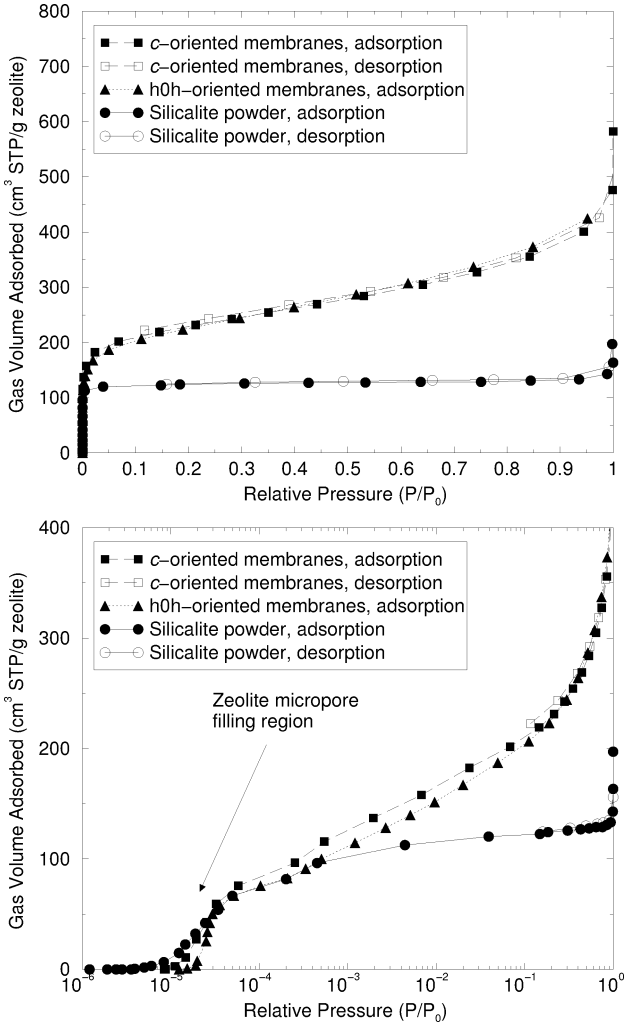

Figure 7. Comparison of argon adsorption isotherms at 77 K for silicalite powder (●), *h*0*h*-oriented silicalite membranes (▲), and *c*-oriented silicalite membranes (■) using mass m_I (obtained by matching the adsorption of membrane and support to powder at the pressure when the micropores are filled). Both linear (top) and logarithmic (bottom) pressure scales are shown.

more consistent at quantitatively matching low-pressure adsorption data between different adsorbates (Table 2): the *h*0*h*-oriented membrane mass from Method (I) differs between argon and nitrogen by 4 mg (well within measurement errors), while the membrane mass from Method (II) differs by 12 mg between nitrogen and argon. Therefore, Method (I) is recommended for estimating the mass of a membrane.

With the masses estimated either by weighing or by the procedure outlined in this section, we seek to determine the quantity adsorbed in the membrane that *cannot* be attributed either to filling micropores in the zeolite or to adsorption in the support. Figures 9 and 10 show the result of calculating a mass-weighted sum of the powder isotherm and the support isotherm, based on the values in Table 2. These hypothetical isotherms are overlaid with the measured one.

4.2. Pore Size Distributions. We estimated the porosity in the membranes using the model of Barrett, Joyner, and Halenda (BJH),[59] which uses the Kelvin equation and an estimate of the thickness of the adsorbed layer to derive a distribution. It should be noted that the Kelvin equation is not accurate for the range of pore sizes relevant in micropores; the concepts of a meniscus and surface tension do not apply at such small length scales. This approach is standard nonetheless and is useful for generating a qualitative picture of pore size distributions. The pore size distribution, using these assumptions, of the silicalite membranes is compared with that of the powder, with the membranes scaled with respect to zeolite mass m_I, to yield the pore size distributions in Figure 11. We also attempted a Saito−Foley[60] (cylindrical pore model) analysis, as well as another based on models tested with nonlocal density functional theory,[61] using the analysis software that accompanies Quantachrome Instruments' AUTOSORB-1,[61] but the results are rather inconsistent and are thus not presented here (see Supporting Information).

4.3. Calculations. We performed flux calculations to gauge the difference between powder and membrane for the purposes of zeolite permeation. A plot of the expected fluxes for the case where the zeolite membrane is on the effluent (vacuum) side is shown in Figure 13. One set of points (open symbols) represents calculations from the argon powder isotherm; filled symbols perform the calculation using membrane measurements. As

(59) Barrett, E. P.; Joyner, L. G.; Halenda, P. P. *J. Am. Chem. Soc.* **1951**, *73*, 373−380.

(60) Saito, A.; Foley, H. C. *AIChE J* **1991**, *37*, 429−436.

(61) Quantachrome Instruments, *AUTOSORB-1 AS1Win Version 1.50 Operating Manual*; Quantachrome Instruments: Boynton Beach, FL, 2004.

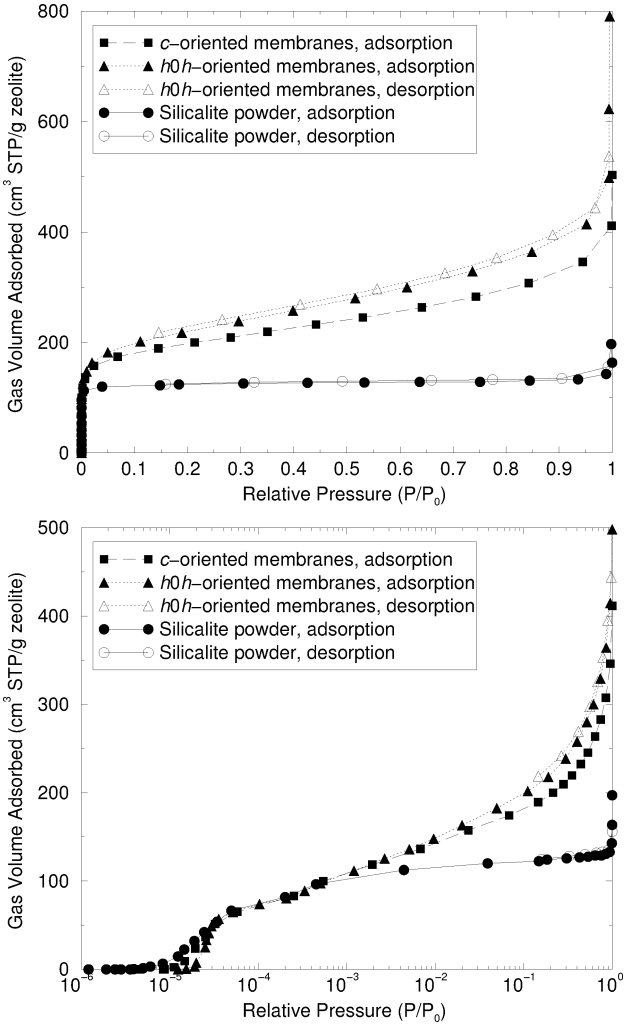

Figure 8. Comparison of argon adsorption isotherms at 77 K for silicalite powder (●), *h*0*h*-oriented silicalite membranes (▲), and *c*-oriented silicalite membranes (■) using mass m_{II} (obtained by matching the adsorption of membrane and support to powder and support in the region between micropore filling and $P/P_0 = 0.1$). Both a linear (top) and logarithmic (bottom) pressure scale are shown.

alluded to in Section 3, we estimate "membrane-only isotherms" by taking the composite isotherms from Figure 7, subtracting the support isotherm from Figure 4, and replacing the region where $d\hat{V}_{ads}/dP < 0$ with a very slightly increasing function as shown in Figure 12. Note that the region near $P/P_0 = 0.01$, where the flux predicted for *c*-oriented membranes increases, is due to the nature of the replacement function: near the point at which the replacement starts, the isotherm is very close to horizontal, meaning $\Gamma = d \log P/d \log \hat{V}$ changes abruptly there and becomes very large. This rapid change in the value of Γ creates increased numerical error, which leads to some inaccuracies in the calculated values.

We examined cases for both *c*- and *h*0*h*-oriented silicalite membranes and found in both cases that unless the diffusion coefficient ($\mathcal{D}$) is much smaller in the zeolite than in the support (by a factor of at least a million), the support's diffusion resistance dominates the calculated value of the flux because of the support's thickness. This can be seen by the fact that the flux is identical for cases where $\mathcal{D}_z$ is smaller than $\mathcal{D}_s$ by a factor of 1000 or smaller in Figures 13 and 14.

The most important observation is that the small domain of relative pressures for which the powder isotherm differs from the membrane isotherm *is not significant to the flux*. To determine whether this is due to the thickness of the membrane relative to the support, we analyzed the case where the support thickness vanishes (that is, $L_s = 0$). As is shown in Figure 15, the flux is *still* not significantly different from one case to the other. We *do* note, however, that the flux through the supported membrane case is about 100 000× smaller than it is for the case without support. This is expected since the support slows down transport through its relative thickness.

We also considered one case (Section 3.4) where we allowed the diffusion coefficient $\mathcal{D}$ to vary according to eq 16. The results from this calculation, which indicate that no significant difference exists between powders and membranes provided the concentration dependence of $\mathcal{D}$ remains the same, are shown in Figures 16 and 17.

5. Discussion

In this work, we set out to answer several questions that are important in understanding adsorption and permeation in zeolite membranes. These include determining the quantity of zeolite present in the membrane or, equivalently, the support/membrane mass ratio; quantifying the extent of mesoporosity in the membrane; comparing membrane and powder isotherms and gauging the importance of discrepancies; and overall, determining whether zeolite membranes exhibit structures that differ from powders.

5.1. Adsorption Analysis. The adsorption isotherms address the questions of support/zeolite ratio, mesoporosity, and powder/zeolite comparisons. As can be seen from Figures 9 and 10, the method of matching powder and membrane adsorption at the "knee" in the high-resolution region to determine the mass and using that mass to add an appropriate mass of powder is a good approximation to the adsorption isotherm of these membranes, which are supported on alumina disc compacts. The adsorption properties of the support comprise a significant fraction of the total amount adsorbed across most of the isotherm for these supported membranes. We also find that the amount adsorbed on the supported membranes at high pressures is *less* than the amount adsorbed on an equivalent amount of support and powder (Figure 10a, for example). This indicates that some of the surface of the support is covered by the zeolite during synthesis, lessening the area available to adsorbate molecules.

The samples analyzed do not display any hysteresis. Hysteresis in the 77 K nitrogen isotherm above 0.42 and the 77 K argon isotherm above 0.18 is a common diagnostic of mesoporosity (pores between 2 and 50 nm). The fact that no hysteresis exists indicates that the pores in the support are much larger than the mesopore range and that any defects in the zeolite must be smaller than 18 Å (the dimension at which the tensile strength effect ceases to contribute to hysteresis).[18] This result is in contrast to the results from other researchers' experiments on unsupported silicalite films, which displayed measurable mesoporosity[19,21−24] (see Supporting Information).

Unlike MFI powders, the membranes we analyzed do not exhibit the low-pressure hysteresis between $P/P_0 = 0.08$ and 0.18 on the nitrogen isotherms. This hysteresis *is* observed in silicalite powder (Figure 3a), and it has also been documented for aluminum-ZSM-5.[62−65] This hysteresis loop was also absent in measurements by Lai and Gavalas,[25] which they attributed to high aluminum content in the membrane. However, this loop is still present in MFI samples that contain aluminum (see Supporting Information), and past experiments with ZSM-5

(62) Kyriakou, G.; Theocharis, C. R. In *Characterization of Porous Solids VI, Stud. Surf. Sci. Catal.* **2002**, *144*, 709−716.

Table 2. Masses of Silicalite Membrane and Support in the Samples, as Determined by High-Resolution Adsorption[a]

sample	total mass (g)	adsorbate	m_I (g)	m_{II} (g)	apparent thickness of zeolite (I/II) (μm)
5 *c*-oriented MFI membranes	7.174	Ar	0.095	0.097	28/29
4 *c*-oriented MFI membranes	5.712	N_2	0.086	0.055	32/21
4 *h*0*h*-oriented MFI membranes	5.789	N_2	0.053	0.046	20/17
4 *h*0*h*-oriented MFI membranes	5.789	Ar	0.057	0.058	21/22

[a] Method (I) matches micropore adsorption; Method (II) matches the powder and support in the $10^{-4}-10^{-2}$ relative pressure range.

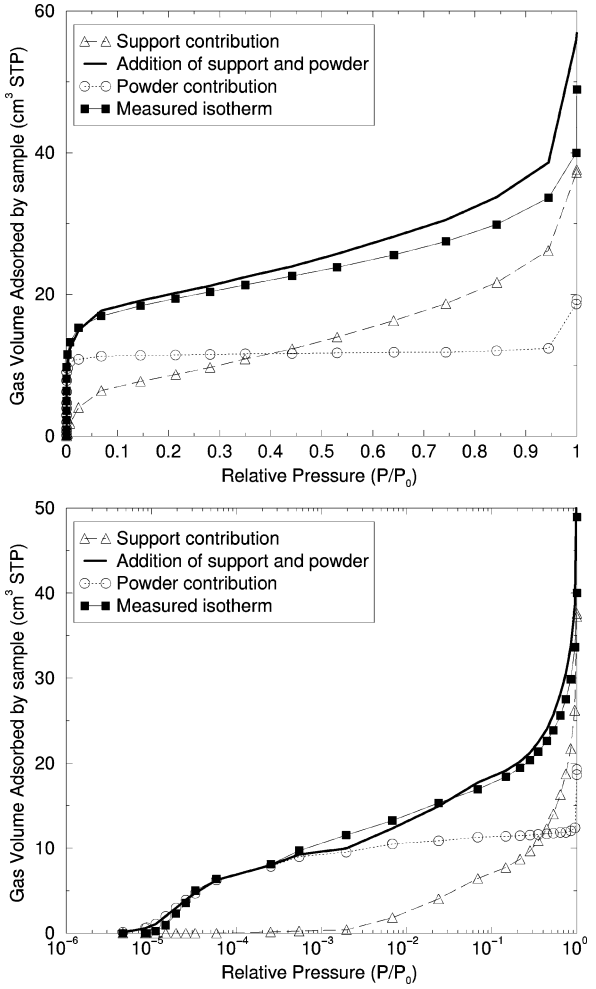

Figure 9. Argon isotherms at 77 K of a *c*-oriented silicalite membrane (■) and the result (thick line) of adding the adsorption isotherm of an appropriate mass (m_I) of silicalite powder (○) and an appropriate mass of support (△). A linear pressure scale is used in the top figure, while a logarithmic pressure scale is used in the bottom figure. Note that the vertical axis has *not* been scaled by mass.

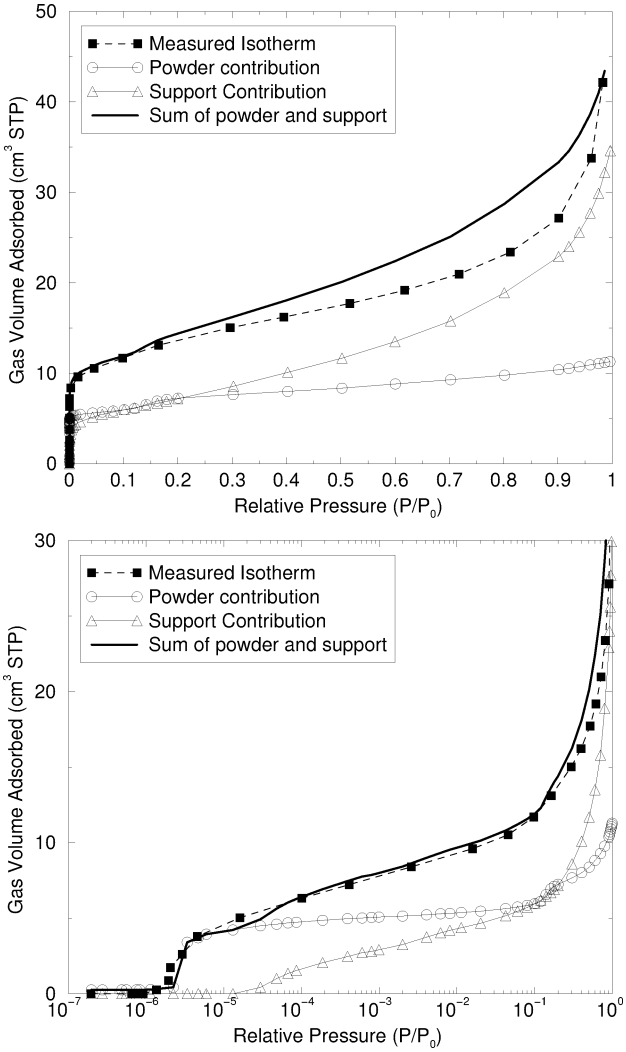

Figure 10. Nitrogen isotherms at 77 K of an *h*0*h*-oriented silicalite membrane. The thick solid line represents the addition of the powder isotherm (Figure 3) to the support isotherm (Figure 4), weighted by the apparent mass m_I of the zeolite (Table 2). The triangles (△) denote the contribution of an appropriate amount of bare support; the circles (○) show the contribution from the powder. Squares (■) denote the actual measured isotherm. Note that the vertical axis has *not* been scaled by mass.

containing aluminum[63−65] showed that this hysteresis is still present in ZSM-5 with fairly high levels of aluminum (up to a silica/alumina ratio of 20:1 in the sample with the highest aluminum content), though its shape changes slightly with aluminum content. In addition, Xomeritakis and co-workers[45] showed that aluminum does not penetrate significantly into silicalite membranes grown by the same technique, so the vast majority of zeolite present in these membranes should be all-silica MFI. In light of this, we suspect this loop is absent in our membrane measurements (and those of others[9,21−25,66,67]) due to structural effects—perhaps the fact that the zeolite crystals cannot expand or contract as much as they can in a powder due to interactions with neighboring crystals in the membrane. This hypothesis is supported by the results of Jeong and co-workers,[50] whose "findings strongly indicate that the MFI crystals on a porous support are no longer the same as those in [a] powder"

(63) Müller, U.; Unger, K. K. In *Characterization of Porous Solids*, *Stud. Surf. Sci. Catal.* **1988,** *39*, 101−108.
(64) Llewellyn, P. L.; Coulomb, J. P.; Grillet, Y.; Patarin, J.; Lauter, H.; Reichert, H. J. R. *Langmuir* **1993**, *9*, 1846−1851.
(65) Llewellyn, P. L.; Coulomb, J. P.; Grillet, Y.; Patarin, J.; Lauter, H.; Reichert, H. J. R. *Langmuir* **1993**, *9*, 1852−1856.
(66) Sakthivel, A.; Jong Huang, S.; Hua Chen, W.; Huang Lan, Z.; Hsien Chen, K.; Wan Kim, T.; Ryoo, R.; Chiang, A. S. T.; Bin Liu, S. *Chem. Mater.* **2004**, *16*, 3168−3175.
(67) Öhrman, O.; Hedlund, J.; Msimang, V.; Möller, K. *Microporous Mesoporous Mater.* **208**, *78*, 199−208.

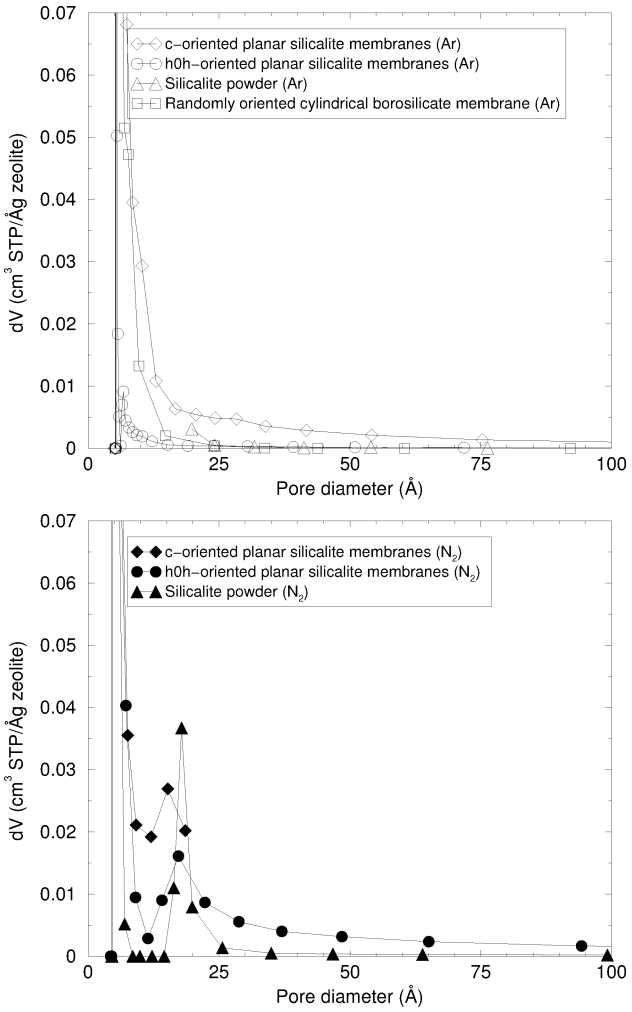

Figure 11. Pore size distributions of supported MFI membranes as determined by the model of Barrett, Joyner, and Halenda.[59] The top figure shows the distribution derived from argon adsorption; the bottom shows the same from nitrogen adsorption. Note that due to the assumptions of the BJH method, the region below 18 Å or so (corresponding to $P/P_0 = 0.42$ for nitrogen) should be interpreted with caution.

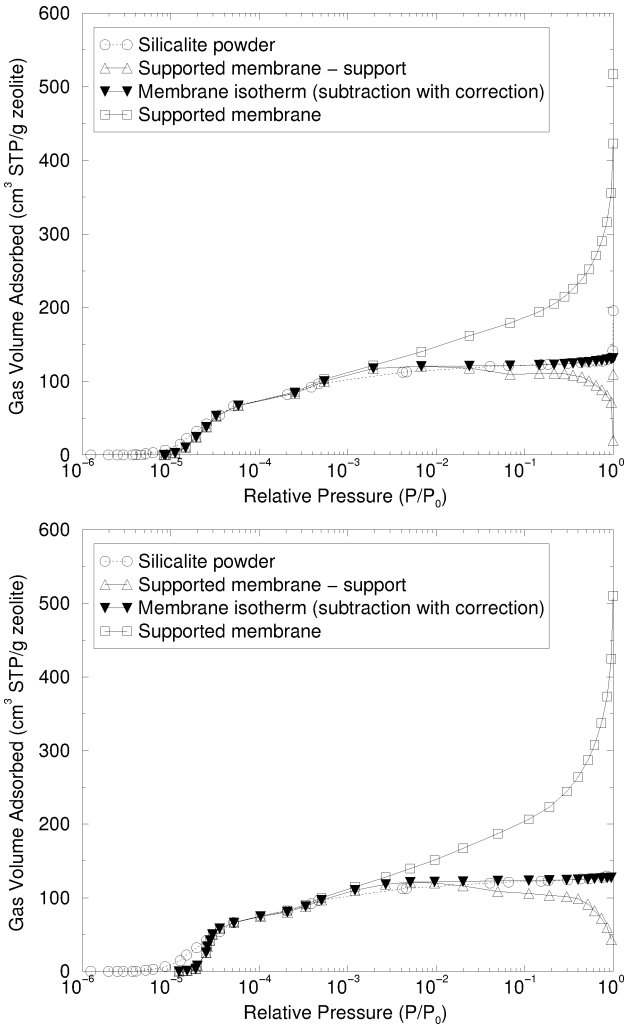

Figure 12. Adsorption isotherms (Ar at 77 K) of *c*-oriented (top) and *h*0*h*-oriented (bottom) zeolite membranes determined by subtracting the support isotherm from that of a supported membrane. The filled symbols denote the corrected isotherms for the membranes themselves (without contributions from the support) that we used in our calculations.

due to stress in the membrane created by the intergrowth, heating/cooling, and calcination processes. The high stresses associated with zeolite membranes often cause cracks to form,[48] and these stresses are highly dependent on the method of fabrication and the rate of cooling.[49] It stands to reason that nonzeolitic porosity may be created and/or destroyed by varying the stress on the membrane.

Pore size distributions are a more quantitative way of assessing the presence of mesopores than mere lack of hysteresis. The pore size distributions obtained based on the Kelvin Equation (Figure 11) are qualitatively similar for all of the samples we examined. This result is in agreement with observations using confocal microscopy: Tsapatsis and co-workers[5,6] showed that membranes grown by the same procedure have detectable crystal defects large enough for moderate-sized molecules (<1 nm kinetic diameter) to enter, but larger defects were not found. The probes in their studies were sodium fluorescein[5] and DCM (4-dicyanomethylene-2-methyl-6-(4-dimethylaminostyryl)-4-*H*-pyran),[6] both of which have a Stokes diameter of ~0.9 nm.[6] The failure of our technique to detect these nonzeolitic micropores indicates that their distribution is relatively broad or their concentration is very low. If either or both of these situations arises, physical adsorption is unlikely to resolve the contribution

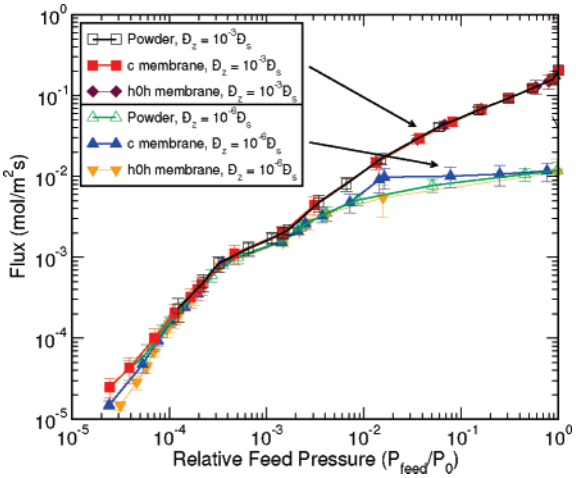

Figure 13. Flux estimate due to surface diffusion with the zeolite membrane on the effluent (vacuum) side. Open symbols represent powder calculations; filled symbols represent membrane calculations.

from such pores due to experimental error. It remains challenging to determine the lowest concentration and broadest size distributions detectable by standard adsorption equipment. One possible

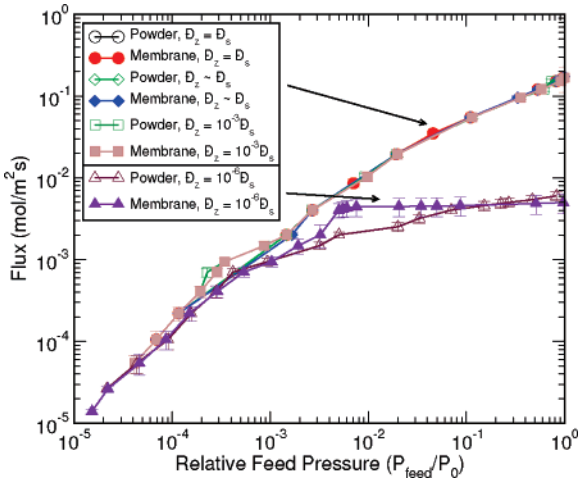

Figure 14. Flux estimate due to surface diffusion with the zeolite membrane on the feed (high-pressure) side. Open symbols represent powder calculations; filled symbols represent membrane calculations.

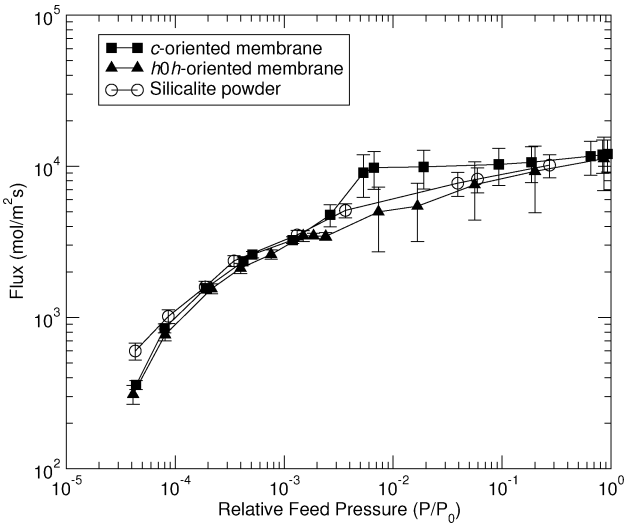

Figure 15. Flux estimate due to surface diffusion for pure zeolite—no support—to compare membranes to powders. The diffusion coefficient in each case was chosen to be 7.5×10^{-7} m^2/s.

way would be to perform a series of experiments wherein silicalite powder is mixed with varying amounts of a mesoporous solid such as MCM-41. If the volume fraction of mesopores in the mesoporous material could be estimated, this would provide a detection threshold for mesoporosity in zeolites. Testing this hypothesis is a target of future research.

It should be noted that 77 K and vacuum are conditions *far* from the conditions normally used for permeation. Although it is possible that room-temperature mesopores may change under stresses associated with cryogenic cooling, thermal expansion coefficients of oxides are on the order of 10^{-6} K^{-1}, likely too small to account for the complete disappearance of mesopores.

5.2. Flux Calculations. Our calculations, using reasonable thicknesses of a membrane and a support as detailed above, examine the assumption that powder and membrane adsorption data are equivalent with respect to their predictions of transport. As Figures 13 and 14 show, the zeolite layer has little or no effect on the flux as a function of feed pressure unless the diffusion coefficient in the support is immense compared to that in the zeolite. Even when the diffusivity ratio ($Đ_s/Đ_z$) is on the order of a million, the difference between support alone and zeolite plus support is only significant at high feed pressures. In no case

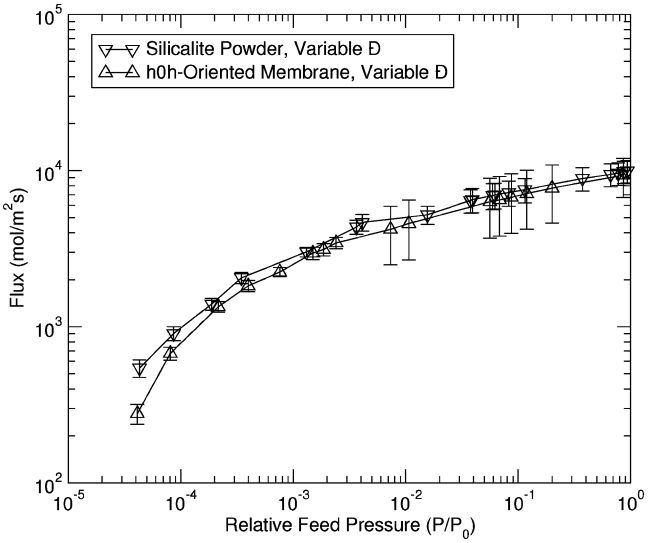

Figure 16. Flux estimate using a concentration-dependent diffusivity according to eq 16a with no support resistance. $Đ_0 = 7.5 \times 10^{-7}$ m^2/s.

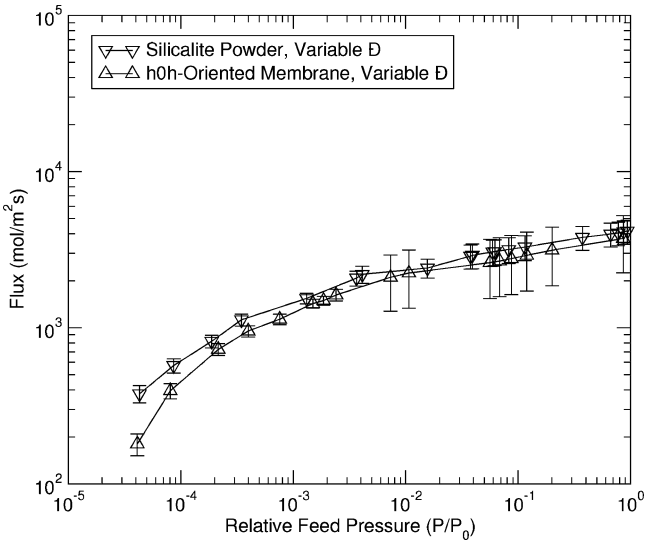

Figure 17. Flux estimate using a concentration-dependent diffusivity according to eq 16b with no support resistance. $Đ_0 = 7.5 \times 10^{-7}$ m^2/s.

did we find that the small differences in adsorption between the powder and the membrane have a significant impact on the flux for this model. We emphasize, however, that this observation must be limited to the membranes studied herein; membranes prepared by significantly different methods (such as membranes where significant mesoporosity *is* present) may show a completely different result.

Assuming that surface diffusion controls membrane permeation, the flux plots indicate the diffusion resistance due to the support is not negligible and may be the controlling factor in the overall flux. This conclusion is contrary to the common preconception that the support's diffusion resistance is negligible compared to that of the zeolite. It is, however, in qualitative agreement with the results of some previous investigations.[68−71] Here, more work is required to quantify the role of the support and to determine the relative importance of other diffusion mechanisms, such as gas-phase (bulk) diffusion and Knudsen diffusion.

(68) van de Graaf, J. M.; van der Bijl, E.; Stol, A.; Kapteijn, F.; Moulijn, J. A. *Ind. Eng. Chem. Res.* **1998**, *37*, 4071−4083.

6. Conclusions

We compare the adsorption properties of intact supported silicalite membranes with those of silicalite powder and of alumina supports using nitrogen and argon as adsorbates at 77 K. We find that silicalite membranes as synthesized as described above can be reasonably approximated by a zeolite powder deposited on a bare support. That is, the adsorption properties of the supported membranes for the purposes of transport can be considered to be the same as a fictitious "supported powder" for the variety of membranes we have investigated. No detectable mesoporosity was found in the membranes, and the minor differences between membranes and powders do not appear to have a significant impact on the calculated flux for this variety of zeolite membrane. We also find that the low-pressure nitrogen hysteresis characteristic of MFI powders at 77 K is *not* present in our membrane samples or those of others; we suggest that this is due to structural constraints in the membrane that are not present in a powder.

Conventional wisdom has been that defects in the membrane are important to permeation in zeolite membranes, but the support is not. The fact that no significant difference between adsorption on powders and adsorption on membranes is observed in this study is a mixed blessing: for scientists attempting to model permeation through membranes such as those studied in this work using measurements from zeolite powders, this work indicates that no significant errors would be expected to be introduced into their models due to porosity in the zeolite. However, this work *also* indicates that ignoring the support probably *will* introduce significant errors into the model.

It may be of interest to repeat the flux calculations presented herein with adsorption measurements using a different temperature and adsorbate (such as benzene,[72−75] xylene,[72] alkanes,[75,76] cyclohexane,[73,74] or hexane[76] near standard temperature) for which experimental flux measurements are available for comparison with the calculations. It would also be of interest to perform these calculations on a membrane that is known to have significant nonzeolitic porosity on the length scale of 2−30 nm; the adsorption isotherms and fluxes for such a membrane would *not* be expected to agree with those of a "supported" zeolite powder.

Nomenclature

Γ	Thermodynamic correction factor, $\partial \log f / \partial \log C$
Γ_s	Thermodynamic correction factor in the support region
Γ_z	Thermodynamic correction factor in the zeolite region
Γ_j	Value of Γ corresponding to $\hat{V}_j$
$(d\Gamma/d\hat{V})_j$	Value of $d\Gamma/d\hat{V}_{ads}$ corresponding to $\hat{V}_j$
ρ_z	Density of the zeolite
θ	Scattering angle (X-ray diffraction)
$\vec{\delta}$	Update vector with elements δ_j
C	Concentration (mol/m^3)
C_{i-edge}	Concentration in region i at the edge of the supported membrane ($x = 0$ or $x = L$)
C_s	Concentration in the support region
C_s^{ads}	Concentration in the support from the adsorption isotherm
C_z	Concentration in the zeolite region
C_z^{ads}	Concentration in the zeolite from the adsorption isotherm
$\mathcal{Đ}$	Maxwell−Stefan diffusion coefficient (m^2/s)
$\mathcal{Đ}_0$	Maxwell−Stefan diffusion coefficient at infinite dilution (zero loading)
$\mathcal{Đ}_s$	Maxwell−Stefan diffusion coefficient in the support layer
$\mathcal{Đ}_z$	Maxwell−Stefan diffusion coefficient in the zeolite layer
D	Fick diffusion coefficient (m^2/s)
F_j	Value of $\mathcal{Đ}/\mathcal{Đ}_0$ at spatial element j
F	Concentration dependence of the corrected diffusivity, equal to $\mathcal{Đ}/\mathcal{Đ}_0$
f	Fugacity of the vapor outside the adsorbent
h	Element spacing
J	Jacobian with matrix elements $J_{ij} = \partial r_i / \partial \hat{V}_j$
L	Thickness of the supported membrane, including the support
L_s	Distance from the bottom edge of the support to the zeolite-support interface
L_z	Distance from the zeolite membrane edge to the zeolite-support interface
L_r	Length of the region in which the diffusion equation is being solved (equal to L_z in the zeolite and L_s in the support)
m_I	Mass (g) of zeolite in the supported membrane(s) as determined by Method I, scaling the membrane isotherm such that it matches the powder at $P/P_0 = 8 \times 10^{-6}$ (N_2) or 6×10^{-5} (Ar)
m_{II}	Mass (g) of zeolite in the supported membrane(s) as determined by Method II, scaling the membrane isotherm such that it matches the *sum* of the powder and support isotherms of the same mass ratio for $P/P_0 \in (10^{-4}, 10^{-2})$.
$\hat{n}_{ads}$	Moles of adsorbed gas in units of moles per gram zeolite
N	Steady-state molar transmembrane flux with respect to fixed coordinates
N^*	Molar flux with respect to fixed coordinates and reduced to have units of standard volume per unit mass
N_s	Steady flux through the support layer
N_z	Steady flux through the zeolite layer
P	Pressure (arbitrary units; usually Torr or Pa)
P/P_0	Relative pressure (unitless)
$P^\ominus$	Standard pressure (1 atm)
P_0	Saturation pressure (arbitrary units; usually Torr or Pa)
P_{i-edge}	Pressure in region i at the edge of the supported membrane ($x = 0$ or $x = L$)
P_s	Pressure in the support from the adsorption isotherm
P_z	Pressure in the zeolite from the adsorption isotherm
$\vec{r}$	Residual vector with elements r_j
R	Universal gas constant
T	Temperature (K)
$T^\ominus$	Standard temperature (298.15 K)
$\hat{V}_{ads}$	Volume of adsorbed gas in units of volume at standard temperature and pressure per gram zeolite
$\hat{V}_j$	Standard volume adsorbed in the supported membrane at spatial element j
x	Position coordinate transverse to the membrane (the direction of permeation)
x^*	Reduced transverse distance coordinate, x/L_r
x_{int}	Location of the interface, equal to L_z if the feed is on the zeolite side and L_s if the feed is on the support side

Acknowledgment. We thank Professor Nair at the Georgia Institute of Technology for synthesizing the membrane samples

(69) van de Graaf, J. M.; Kapteijn, F.; Moulijn, J. A. *J. Membr. Sci.* **1998**, *144*, 87−104.
(70) Jareman, F.; Hedlund, J.; Creaser, D.; Sterte, J. *J. Membr. Sci.* **2004**, *236*, 81−89.
(71) Lai, Z. P.; Tsapatsis, M.; Nicolich, J. R. *Adv. Func. Mater.* **2004**, *14*, 716−729.
(72) Gump, C. J.; Tuan, V. A.; Noble, R. D.; Falconer, J. L. *Ind. Eng. Chem. Res.* **2001**, *40*, 565−577.
(73) Jeong, B.-H.; Hasegawa, Y.; Kusakabe, K.; Morooka, S. *Sep. Sci. Technol.* **2002**, *37*, 1225−1239.
(74) Nikolakis, V.; Xomeritakis, G.; Abibi, A.; Dickson, M.; Tsapatsis, M.; Vlachos, D. G. *J. Membr. Sci.* **2001**, *184*, 209−219.
(75) Jeong, B.-H.; Hasegawa, Y.; Sotowa, K.-I.; Kusakabe, K.; Morooka, S. *J. Chem. Eng. Jpn.* **2002**, *35*, 167−172.
(76) Jeong, B.-H.; Hasegawa, Y.; Sotowa, K.-I.; Kusakabe, K.; Morooka, S. *Ind. Eng. Chem. Res.* **2002**, *41*, 1768−1773.

we analyze in this paper. We also thank the referees for their helpful comments and suggestions. K.D.H. thanks Professor Maroudas at UMass Amherst for helpful teaching and guidance with the calculations and the Watkins group at UMass Amherst for the use of their oven for firing supports. The authors are most grateful to the United States Department of Energy (DE−FG02−94ER14485) for its generous funding of this research.

Supporting Information Available: Additional data and figures. This material is available free of charge via the Internet at http://pubs.acs.org.

LA063256C